Effect of Tank Size and Geometry on the Flow Induced by Circular Bubble Plumes and Water Jets

Iran E. Lima Neto[1]; David Z. Zhu, M.ASCE[2]; and Nallamuthu Rajaratnam, F.ASCE[3]

Abstract: Ambient flow field and circulation patterns induced by circular bubble plumes and water jets in tanks of different sizes were studied in rectangular and square water tanks. A nonstationary nature of the flow was observed in all experiments and its dominant oscillation frequency was found to directly relate to the tank size. The flow circulation patterns were similar for bubble plumes and water jets, but changed significantly with tank size and geometry. Strong three-dimensional effects were observed in a rectangular tank, resulting in flow entraining in the longer plane and flow detraining in the shorter plane, especially for the bubble plume tests. A relationship was developed to relate the tank size to the patterns of circulation cells. Nearly isotropic turbulent flow conditions were obtained in all experiments, but the effect of tank size and geometry on the magnitude of the turbulent stresses was more pronounced in the bubble plume tests.

DOI: 10.1061/(ASCE)0733-9429(2008)134:6(833)

CE Database subject headings: Bubbles; Water circulation; Water tanks; Water jets; Mixing; Plumes; Geometry; Turbulent flow.

Introduction

Bubble plumes and water jets are widely used to promote circulation and turbulent mixing in aeration tanks, mixing chambers, reservoirs, lakes, and other water bodies (Abramovich 1963; Rajaratnam 1976; Socolofsky 2001; Soga and Rehmann 2004). While bubble plumes entrain the surrounding liquid mainly due to buoyancy, water jets induce the entrainment mainly due to momentum. Earlier studies have mostly focused on the dynamics of jets and plumes. Only a few studies examined the effects of the tank sizes and geometry on the ambient flows and circulations patterns (Iamandi and Rouse 1969; Jirka and Harleman 1979; Fanneløp et al. 1991; Riess and Fanneløp 1998).

Iamandi and Rouse (1969) studied plane air jets in tanks with different lengths and found that a primary circulation flow cell was formed when this length was up to about two times the height of the tank. However, a secondary cell with opposite rotation of the primary cell was also formed when the length of the tank was four times its height. In this particular case, the length of the primary cell was about 2.5 times the height of the tank. Jirka and Harleman (1979) investigated buoyant plane water jets with different lengths and water depths and found that circulation cells were formed when the discharge was unstable. But, in contrast with the above-mentioned nonbuoyant case, no secondary cell was formed even when the length of the tank was about 20 times the water depth. Fanneløp et al. (1991) and Riess and Fanneløp (1998) studied plane water jets and line-source bubble plumes and observed the formation of secondary cells in water tanks with a length of about 20 times the water depth. Nevertheless, the length of the primary cell was about seven times the water depth, which is much larger than that reported by Iamandi and Rouse (1969). In all the above studies, line jets and plumes were used across the channel width; thus, the flows were made two-dimensional (2D) without three-dimensional (3D) effects.

The flow field induced by bubble plumes in confined setups such as bubble column reactors has also been investigated. Experimental studies have shown that the number of vertical circulation cells generated in these setups is close to the ratio of column height to diameter or width (see the summary in Mudde 2005). However, no general description of the effect of tank size and geometry, ranging from confined setups to larger scale tanks, has been provided.

In both confined and unconfined bubble plume setups, a periodic lateral oscillation of the bubble core (also called wandering motion) is usually reported (Rensen and Roig 2001; García and García 2006). Rensen and Roig (2001) studied the wandering motion in a confined bubble column and obtained oscillation frequencies ranging from about 0.1 to 0.2 Hz, increasing with the air flow rate following approximately a power law with a slope of about 0.50. García and García (2006), on the other hand, studied the wandering motion in a large wastewater treatment tank and obtained much smaller oscillation frequencies (ranging from about 0.002 to 0.003 Hz). They noticed that the frequencies in-

[1]Ph.D. Candidate, Dept. of Civil and Environmental Engineering, Univ. of Alberta, Edmonton AB, Canada T6G 2W2. E-mail: limaneto@ualberta.ca

[2]Professor, Dept. of Civil and Environmental Engineering, Univ. of Alberta, Edmonton AB, Canada T6G 2W2 (corresponding author). E-mail: david.zhu@ualberta.ca

[3]Professor Emeritus, Dept. of Civil and Environmental Engineering, Univ. of Alberta, Edmonton AB, Canada T6G 2W2. E-mail: nrajaratnam@ualberta.ca

Note. Discussion open until November 1, 2008. Separate discussions must be submitted for individual papers. To extend the closing date by one month, a written request must be filed with the ASCE Managing Editor. The manuscript for this technical note was submitted for review and possible publication on February 15, 2007; approved on June 26, 2007. This technical note is part of the ***Journal of Hydraulic Engineering***, Vol. 134, No. 6, June 1, 2008. ©ASCE, ISSN 0733-9429/2008/6-833–842/$25.00.

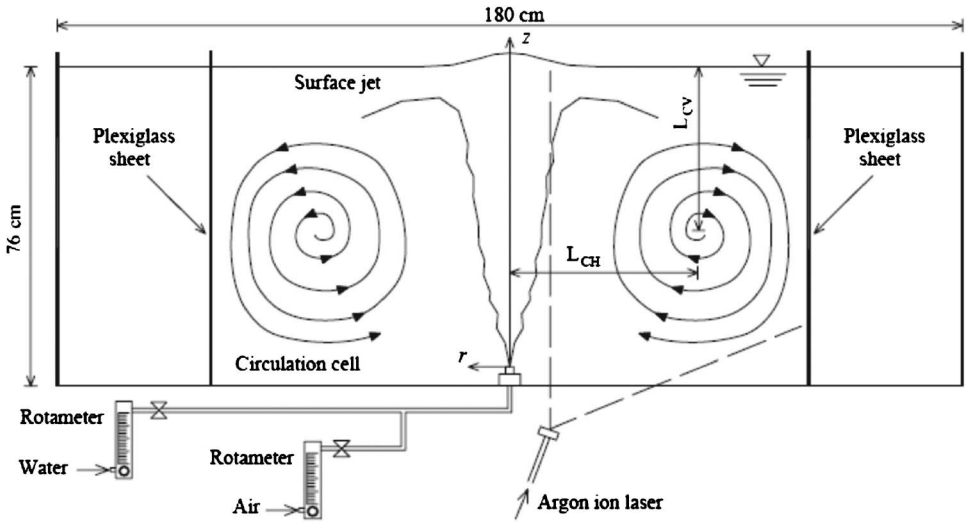

Fig. 1. Schematic of experimental apparatus, indicating circulation flow cells at the longer side of the rectangular tank with two plexiglass sheets (for the square setup). Note that the confined setup (not shown in the figure) was obtained by placing a plexiglass box at the center of the tank.

creased with the air flow rate following approximately a power law with a slope of about 0.30. This implies that the wandering frequency depends on both tank size and air flow rate, but no general correlation including both small and large scale tanks has been provided. Besides, there remain debates on the mechanism that cause this oscillatory flow, either attributing it to buoyancy-driven instabilities enhanced by the presence of the walls and/or the presence of coherent flow structures. Therefore, measurements of the mean, turbulent, and periodic flows induced by bubble plumes and water jets for different tank geometries are necessary to improve knowledge of such flows and to validate computational fluid dynamic codes using advanced techniques such as large-eddy simulation (see Bombardelli 2004).

In the present study we investigate experimentally the effect of tank size and geometry, including rectangular and square setups, on the mean, turbulent, and periodic flow fields induced by circular bubble plumes and water jets. We analyzed our results and combined them with those available in the literature to provide a better understanding of such flows.

Experimental Setup and Procedure

The experiments were performed using three different setups: a rectangular tank, a square tank, and a smaller square tank (here called a confined setup), shown schematically in Fig. 1. The rectangular setup consisted of a glass-walled tank, 1.20 m wide, 1.80 m long, and 0.80 m deep. The square setup was built by placing two plexiglass sheets inside the rectangular tank to form a 1.20-m square tank. The confined setup was obtained by placing a plexiglass box of a 0.40-m side at the center of the tank in order to reach similar conditions as bubble columns. The water depth was fixed at 0.76 m for all setups. The gas supply was taken from an air line, while the water was pumped from a small reservoir. Both air and water temperatures were about 20°C. Volumetric flow rates of 33.3 and 50.0 cm^3/s were adjusted by rotameters for both the air and water phases (a total of four experiments for one tank geometry) and discharged through single-orifice nozzles connected to the air and water lines by a PVC pipe with an inner diameter of 25.4 mm. A pressure-regulating valve was used to keep the air pressure at 1 ATM to ensure a constant air flow rate to the nozzle during the bubble plume tests. The diameter of the nozzles, d_o, used in the air and water injection tests were 1.5 and 3.0 mm, respectively. The nozzles were placed at the center of the tank and their exit was 45 mm above the bottom. The experiments with water injection were limited to the square and rectangular setups to minimize the effect of increase in the water level, which was less than 1% over the duration of the experiments in both cases. These flow rates and nozzle diameters were chosen in order to provide similar velocity scales of the entrained liquid jet for the air and water injection tests. Table 1 shows a summary of the experimental conditions, the Reynolds number being defined as $R=U_o d_o/\nu$, where U_o and ν=velocity at the nozzle exit and kinematic viscosity for each phase (air or water), respectively.

Typical images of the bubble plumes and water jets are shown in Fig. 2. A spreading rate of about 20% of the height is observed by injecting dye close to the nozzle exit (for bubble plumes) and at the water supply pipeline (for water jets). In the bubble plume

Table 1. Details of Experimental Conditions, Showing Centerline Velocities Measured with the Propeller Anemometer at 40 cm above the Nozzle Exit for the Square and Rectangular Setups

Condition	Square (1.2 m×1.2 m)	Rectangular (1.2 m×1.8 m)	Confined (0.4 m×0.4 m)	Air and water flow injection rates
Bubble plume (d_o=1.5 mm)	×	×	×	Q_o=33.3 cm^3/s, U_o=18.9 m/s, R=1,885, $U_{c,40\ cm}$=24 cm/s
				Q_o=50.0 cm^3/s, U_o=28.3 m/s, R=2,831, $U_{c,40\ cm}$=32 cm/s
Water jet (d_o=3.0 mm)	×	×		Q_o=33.3 cm^3/s, U_o=4.7 m/s, R=14,140, $U_{c,40\ cm}$=20 cm/s
				Q_o=50.0 cm^3/s, U_o=7.1 m/s, R=21,231, $U_{c,40\ cm}$=29 cm/s

Note: Water depth was fixed at 0.76 m in all experiments.

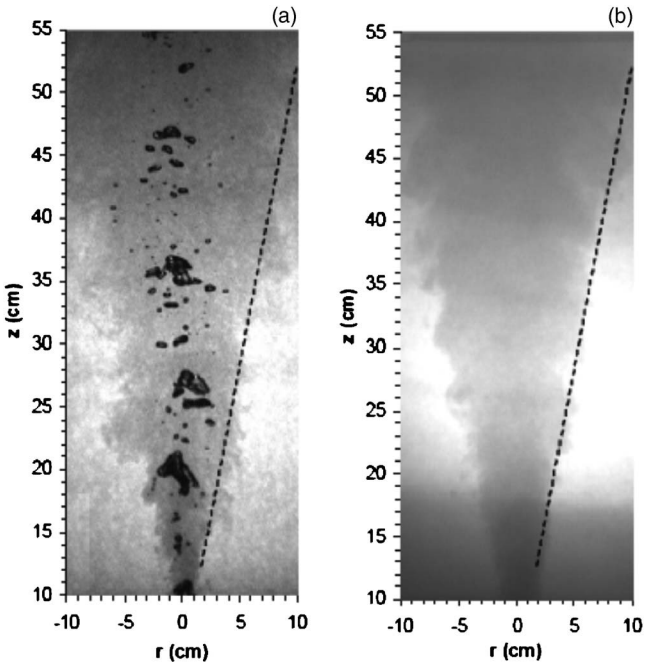

Fig. 2. Typical images obtained using background illumination and dye injection: (a) bubble plumes; (b) water jets (Q_o=33.3 cm^3/s). Dashed line indicates a 20% spreading with height.

tests, the ratio of the bubble core to the entrained liquid jet diameter was about 0.6, which was within the typical range of 0.5–0.9 reported by Socolofsky (2001). Therefore, the bubble core had a spreading rate of about 12%. An electromagnetic propeller anemometer (Omni Instruments, MiniWater20) with an internal diameter of 22 mm was used to measure mean vertical water velocity inside the bubble plumes and water jets in the square and rectangular setups. The measured velocities at the centerline water jet at different distances above the nozzle were about 10% smaller than those obtained by using the classical theory of free jets (see Rajaratnam 1976). This 10% difference was probably due to the accuracy of the propeller anemometer, as well as the assumption of the jet behaving like an ideal jet. Table 1 shows that although the velocity at the nozzle exit, U_o, for bubble plumes was higher than that for water jets, the centerline water velocity measured with the propeller anemometer at 0.40 m above the nozzle exit, $U_{c,40\ \mathrm{cm}}$, was of the same order. The small Reynolds number in the bubble plume tests also ensured that the flow was dominated by buoyancy forces. The bubble plumes contained bubbles of mean volume equivalent-sphere diameters of about 8 mm, which were measured across the bubble core at 0.40 m above the nozzle exit using an optical probe system described by Lima Neto et al. (2008). Visual observation of the bubble plumes and the entrained fluid (from dye injection tests) in the square and rectangular setups revealed a low-frequency oscillation of the core (wandering motion), which was smaller than that observed in the confined setup. This wandering frequency also appeared to increase with air flow rate. The water jets, however, did not present significant wandering motions.

The flow field surrounding the bubble plumes and water jets was measured using particle image velocimetry (PIV). Silver-coated glass particles with a density of 1.65 g/cm^3 and a mean diameter of 15 μm were homogenously distributed into the water. A continuous 6 W argon ion laser operating at 488 nm (Stabilite 2017, Spectra-Physics Lasers) and optics (OZ optics) were used to generate a light sheet to illuminate the flow (see Fig. 1). Because strong 3D effects were observed in the rectangular setup for both bubble plumes and water jets, measurements were taken both in the longer and shorter planes of the tank. A high-resolution charge-coupled device (CCD) camera (1392 × 1040 pixels) (TM-1040, Pulnix America, Inc.) controlled by a computer frame grabber system (Streams 5, IO Industries, Inc.) captured 10-bit images of the particles with a resolution of

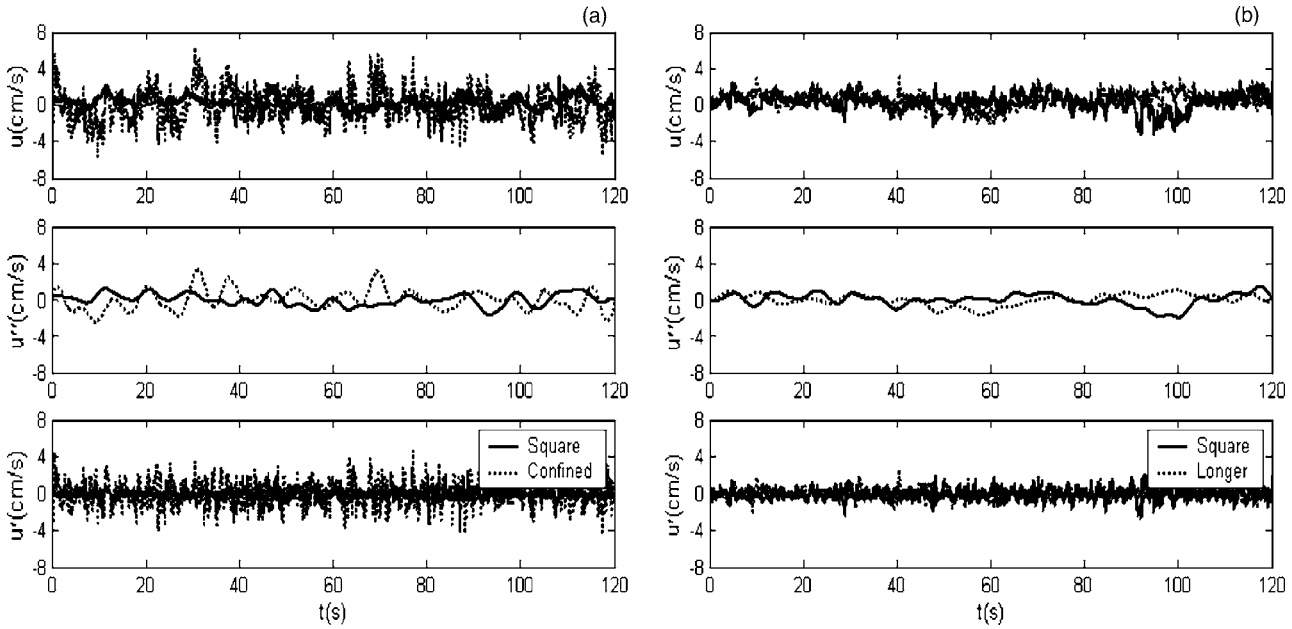

Fig. 3. Instantaneous horizontal velocity (u) measured at r=15 cm and z=40 cm (Q_o=33.3 cm^3/s), periodic component (u''), and turbulent component (u'), for the flow induced by (a) bubble plumes in the square and confined setups; (b) water jets in the square and rectangular (in the longer plane) setups

J. Hydraul. Eng., 2008, 134(6): 833-842

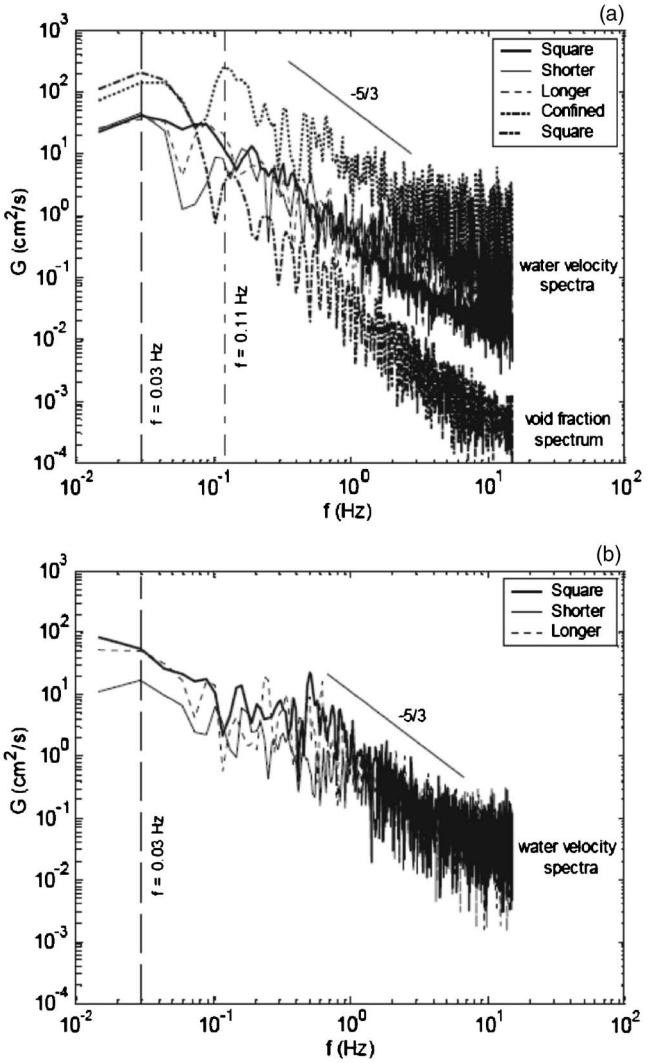

Fig. 4. Power spectra of horizontal velocity component u measured at $r=15$ cm and $z=40$ cm for the square, rectangular (in both shorter and longer planes), and confined setups, indicating dominant frequencies of about 0.03 and 0.11 Hz and the presence of an inertial subrange (line with slope of $-5/3$): (a) bubble plumes (also indicating a void fraction spectrum for the square setup measured at $r=0$ cm and $z=40$ cm); (b) water jets ($Q_o=33.3$ cm^3/s)

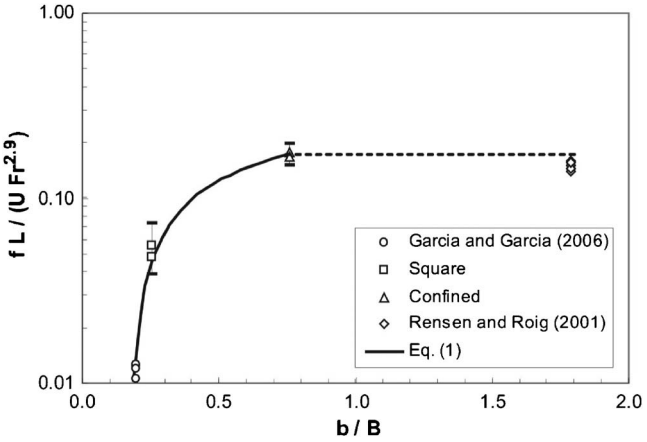

Fig. 5. Variation of the dimensionless wandering frequency with the ratio of jet radius to tank radius (or half-width). Our data points correspond to the air flow rates Q_o of 33.3 and 50.0 cm^3/s, including the 95% confidence intervals (indicated with error bars). Dashed line indicates the region where the wandering frequency becomes independent of b/B, according to the experimental results of Rensen and Roig (2001).

18 pixel/cm, frame rate of 30 fps, and exposure time of 1/60 s for all setups. The displacements between subsequent images were computed using a standard cross-correlation PIV algorithm (Heurisko, version 4.0.8, Aeon Verlag and Studio) with an interrogation window size of 32×32 pixels and 50% overlap between adjacent windows. In the confined setup, because of the wandering motion and the proximity of the PIV field of view to the bubble core centerline (7 cm), a few bubbles could be periodically observed (closer to the water surface), but this effect was considered negligible as the PIV code corrected the velocity vectors using a threshold technique. This problem was much less pronounced in the square and rectangular setups, where the frequency of the wandering was lower and the PIV field of view was located farther away from the bubble core centerline (10 cm).

The bubble plume experiments were performed for 2 and 5 min in duration, which resulted in similar flow patterns. This is consistent with preliminary bubble plume tests in the square setup conducted by Lima Neto et al. (2008) with sampling times ranging from 5 to 30 min, which resulted in measurements of average air-phase properties (void fraction, bubble velocity, and diameter) within only about a 10% difference. We decided not to exceed the 2 min duration in the water jet tests in order to minimize the effect of increasing water level in the tank.

Results and Discussions

Typical horizontal velocity components, u, obtained from PIV measurements of the flow near the bubble plumes and water jets, and power spectrums of these velocities, G_u, are shown in Figs. 3 and 4, respectively. In Fig. 4, a line with a slope of $-5/3$ is also shown to indicate the presence of Kolmogorov's inertial subrange. A dominant frequency, f, of about 0.03 Hz was obtained for the velocity signals near the core of both the bubble plumes and water jets in the square and rectangular setups. The same frequency was obtained for different sampling times (2 and 5 min) and from optical probe measurements of void fraction (5 min duration) at the bubble core centerline in the square setup. Thus, the dominant frequency in the spectrum of bubble plumes will be considered here as a wandering frequency, as suggested by Rensen and Roig (2001). A dominant frequency of about 0.11 Hz was obtained for the velocity signals near the bubble core in the confined setup and it was also considered as a wandering frequency for this particular case. This is consistent with the higher wandering frequency observed visually in the confined setup. Note that these frequencies were obtained for the flow rate of 33.3 cm^3/s. For the higher flow rate used in this study (50.0 cm^3/s), these frequencies were higher, i.e., about 0.04 for the square/rectangular setups and 0.12 Hz for the confined setup. This supports the idea that these dominant frequencies corresponded to the wandering frequencies of the bubble plumes, which increased with air flow rate but decreased with tank size. It is important to mention, however, that estimation of the 95% confidence intervals in the power spectra shown in Fig. 4 resulted in deviations of the peak frequency by up to about 33%. In this case, the peak frequencies for 33.3 and 50.0 cm^3/s will be assumed to be of the same order. Visual observation and optical

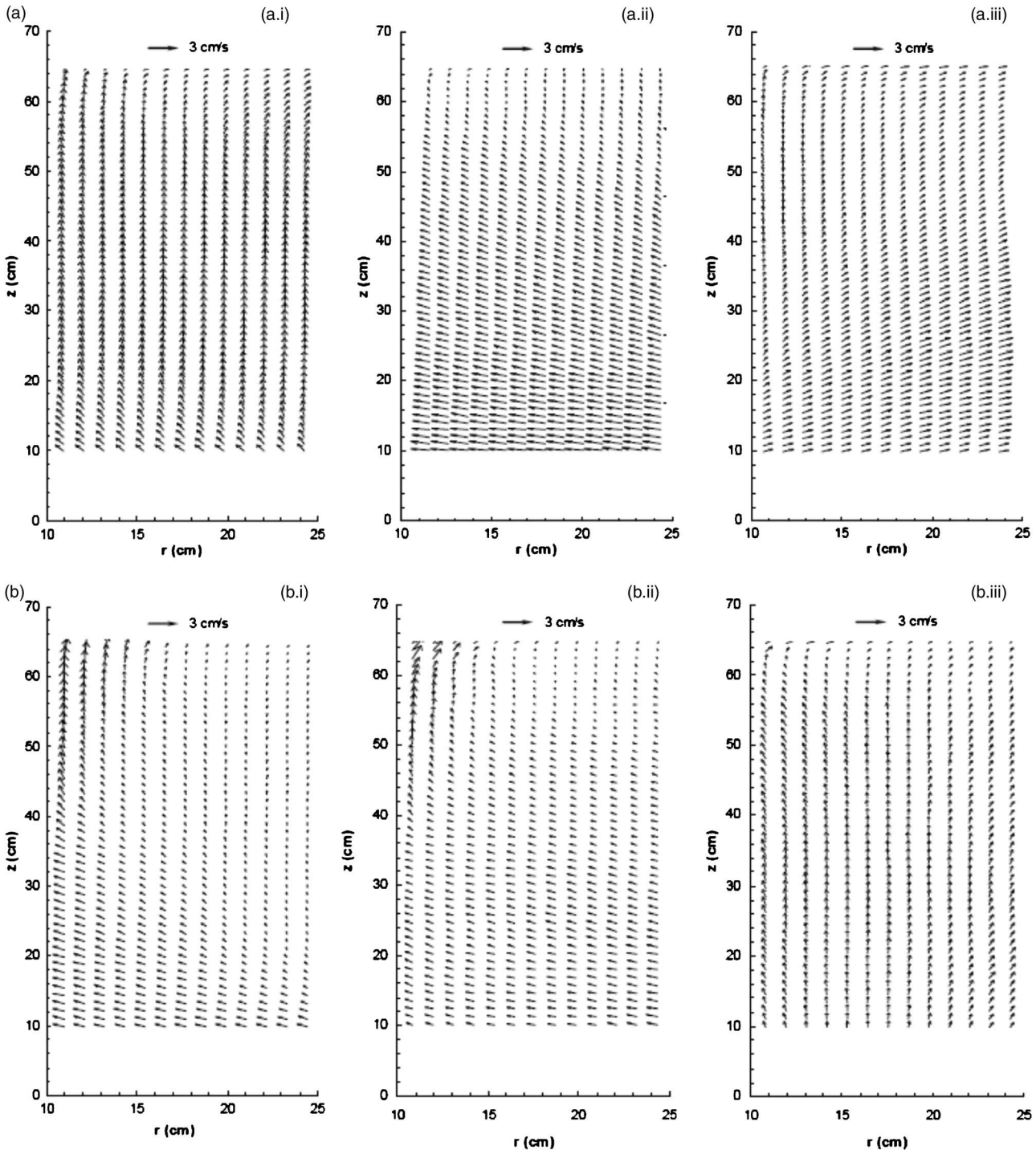

Fig. 6. Time-averaged velocity fields surrounding the (a) bubble plumes; (b) water jets in the (i) square setup, (ii) longer, and (iii) shorter planes of the rectangular setup (Q_o=33.3 cm^3/s). Note that the mean vertical velocity $\bar{v}$ is distorted (about 3.5 times smaller).

probe measurements of the bubble core oscillation also confirmed a weak influence of the air flow rate tested here on the wandering motion, as compared to that of tank size.

Because of the nonstationary nature of the flow, a digital filtering technique was used to separate the turbulent motions (i.e., high-frequency signals) and the periodic motions (i.e., low-frequency signals) from the original velocity signals. In order to define a cutoff frequency, we examined the coherence between the horizontal and vertical velocity components, estimated using the power spectra of these variables. Thus, a low coherence indicates the random (i.e., turbulent) motions while a high coherence indicates the well correlated (i.e., periodic) motions. A frequency of 0.2 Hz gave a coherence lower than about 0.3 for the high-frequency signals and a coherence higher than about 0.7 for the low-frequency signals. Although some contamination between the turbulent and periodic motions is expected in the above procedure, the use of 0.2 Hz as a cutoff frequency fitted very well with the periodic velocity fluctuations in the instantaneous velocity time series. This is also consistent with the procedure described by García and García (2006), where a cutoff frequency higher

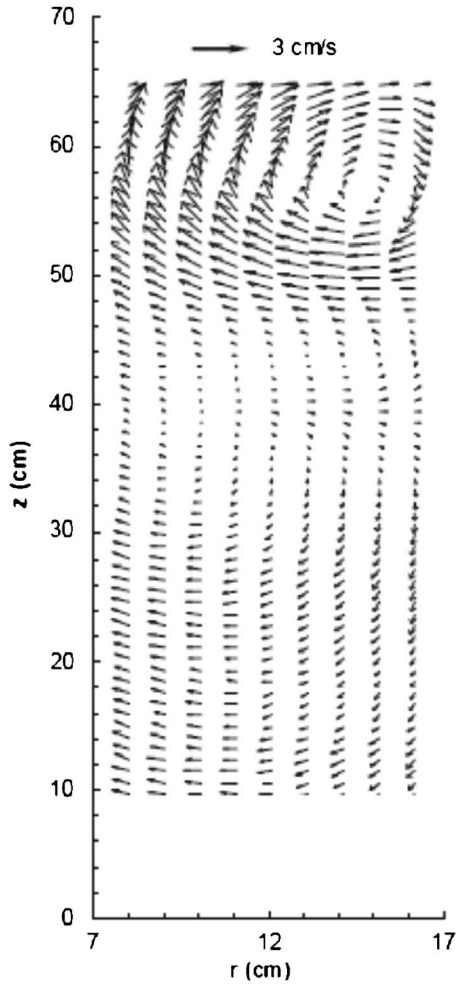

Fig. 7. Time-averaged velocity field surrounding the bubble plumes in the confined setup (Q_o=33.3 cm^3/s). Note that the mean vertical velocity $\bar{v}$ is distorted (about 3.5 times smaller).

than the dominant wandering frequency was used to decompose the velocity signals. Hence, considering this cutoff frequency, sixth-order Butterworth high-pass filters were used to eliminate the mean velocities ($\bar{u}$ and $\bar{v}$) from the original velocity signals (u and v) and separate the dominant periodic velocity fluctuations (u'' and v'') from the turbulent velocity fluctuations (u' and v'), where $u=\bar{u}+u'+u''$ and $v=\bar{v}+v'+v''$. Examples of this velocity decomposition are shown in Fig. 3. It is seen that both u'' and u' in the confined setup are higher than those for the square and rectangular setups.

To examine the effect of the tank size on the dominant frequency (or wandering frequency) induced by bubble plumes and to nondimensionalize the results, we introduce the ratio b/B, where b=length scale for the jet and plume at the free surface and B=tank radius or half-width. For circular jets and plumes, b can be estimated as $b=0.2H$ (Rajaratnam 1976), where H=travel distance of the jet and plume to the water surface. To examine the effect of the air flow rate, we introduce velocity and length scales defined by $U=Q_o/L^2$ and $L=(Q_o^2/g)^{1/5}$, respectively, as well as a densimetric Froude number defined by $\mathrm{F}=U/\sqrt{bg(\rho_w-\rho_a)/\rho_w}$, in which ρ_w and ρ_a=water density and air density, respectively. Thus, combining the above parameters with curve fitting of experimental data obtained here and available in the literature, a dimensionless wandering frequency can be expressed by the following equation:

$$\frac{fL}{U}=\mathrm{F}r^{2.9}\left[0.268\log\left(\frac{b}{B}\right)+0.205\right] \quad (1)$$

Fig. 5 shows that Eq. (1) describes well (r^2=0.994) the experimental data and that the dimensionless wandering frequency fL/U increases as the tank size becomes small compared to the jet radius up to b/B=0.76, where this frequency becomes independent of tank size. This is consistent with the experimental results of Rensen and Roig (2001), in which the wandering frequency was constant for b/B varying from about 0.7 to 1.8. It is interesting to note that, according to Eq. (1), the wandering frequency also increases with the air flow rate following approximately a power law with a slope of 0.38, which is within the above-mentioned values of 0.30 and 0.50 obtained from the data given by Rensen and Roig (2001) and García and García (2006).

The comparison shown in Fig. 5 is for bubble plume studies with different diffusers but similar range of bubble diameters: 3 mm (obtained from Rensen and Roig 2001); 8 mm (obtained from the present study); and 10 mm (estimated for the coarse bubble diffuser used by García and García 2006). Note that these bubble diameters are within the range of 1–15 mm reported by Clift et al. (1978) for ellipsoidal bubbles. Previous study by Lima Neto et al. (2008) on bubble plumes generated using different nozzle types (including single and multiple orifices of different sizes and a porous airstone) resulted in similar wandering frequencies as obtained in the present study, even though the average bubble diameters varied from 3 to 10 mm with different nozzle types. In addition, all the data presented in Fig. 5 correspond to studies with diffusers occupying a small area on the bottom of the tank, which can be assumed to be point-source diffusers. Therefore, we expect that Eq. (1) should be valid for those types of diffusers and the above-mentioned bubble sizes.

Similar flow patterns surrounding the bubble plumes and water jets were obtained for both volumetric flow rates (33.3 and 50.0 cm^3/s). Typical time-averaged flow fields for the square and rectangular setups are shown in Fig. 6. It can be seen that the time-averaged horizontal velocity component, $\bar{u}$, decreased with height while the vertical velocity component, $\bar{v}$, increased until the flow approached the surface jet region, as observed by Fanneløp et al. (1991) and Riess and Fanneløp (1998) for line-source bubble plumes. However, in our bubble plume tests, strong 3D effects were generated in the rectangular tank, with larger water flow entraining in the longer plane and smaller water flow detraining in the shorter plane. Similar 3D effects were generated in our water jet tests, with water flow entraining in the longer plane and part of the flow entraining (up to about r=15 cm) and then detraining in the shorter plane. This implies that the bubble plumes were more affected by the tank asymmetry than the water jets.

A time-averaged flow field for the bubble plumes in the confined setup is shown in Fig. 7, in which more than one circulation flow cell (vortex) was generated, in contrast with the above-mentioned flow patterns for bubble plumes in the square and rectangular setups. The presence of about two vortices stacked vertically in the confined setup is consistent with the results summarized by Mudde (2005), in which the number of vertical cells is close to the aspect ratio $H/2B$ (note that in our case $H/2B$ =1.9).

Fig. 8 shows large-circulation patterns for each plane of the square and rectangular setups in which the entraining and detrain-

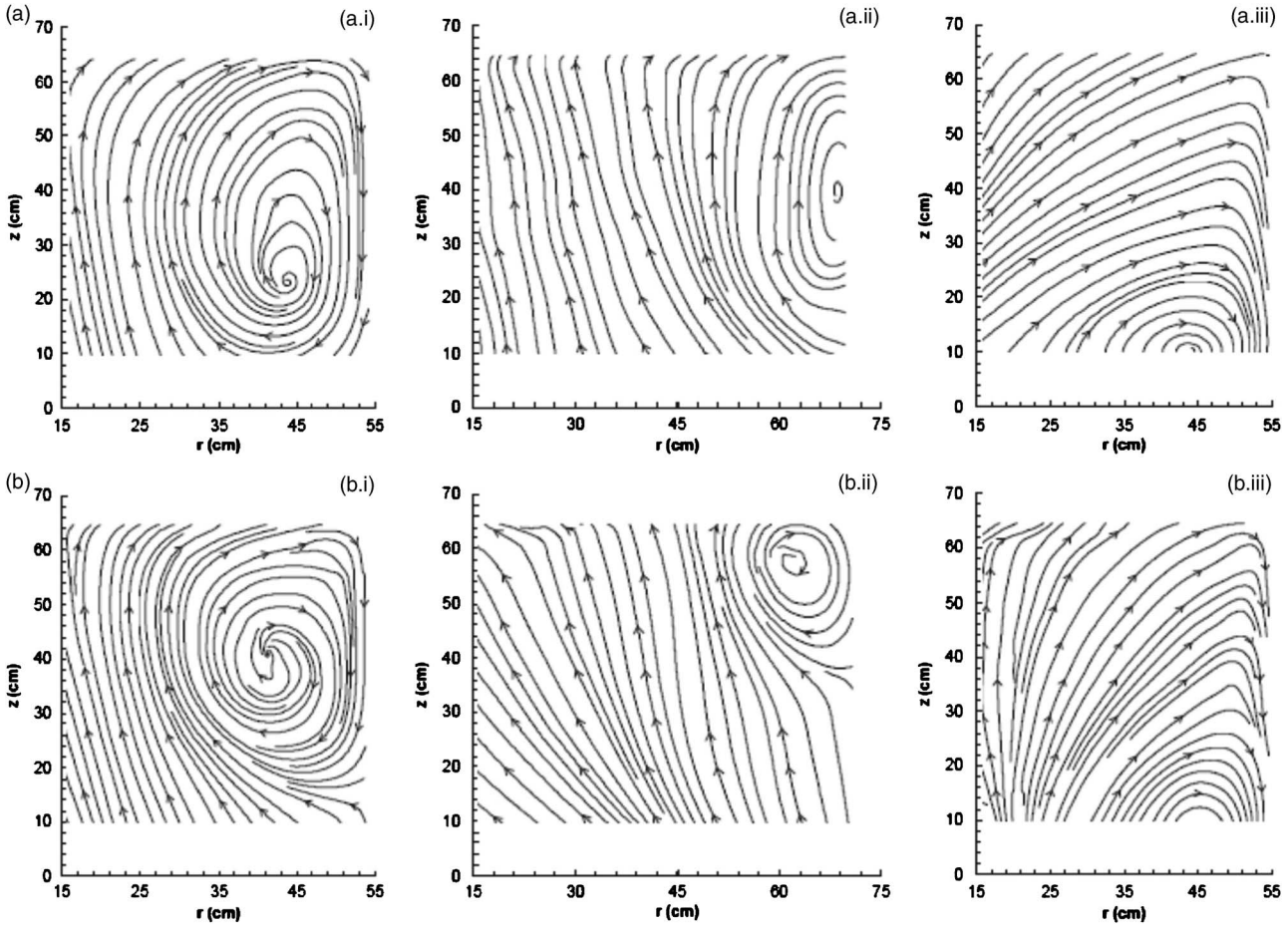

Fig. 8. Streamlines generated from time-averaged PIV measurements for the flow surrounding the (a) bubble plumes; (b) water jets in the (i) square setup, (ii) longer, and (iii) shorter planes of the rectangular setup (Q_o=50.0 cm^3/s)

ing flows are clearly represented through streamlines generated from PIV measurements. The flow patterns obtained for the bubbles plumes were similar to those obtained for the water jets, with the center of the circulation cells located approximately at the same positions. However, the center of the circulation cells in the longer plane of the rectangular setup was much closer to the water surface, while in the shorter plane it was closer to the tank bottom. Comparing these flow patterns with that shown in Fig. 7, we can see that both the number of cells and location of their centers varied with tank size and geometry.

The presence of large-circulation flow cells surrounding the bubble plumes and water jets (see Fig. 8) is consistent with the length of the cells varying from about two to seven times the water depth reported by Iamandi and Rouse (1969), Jirka and Harleman (1979), Fanneløp et al. (1991), and Riess and Fanneløp (1998). This suggests that tank aspect ratios $H/2B$ lower than about 0.25 are necessary to generate more than one circulation cell in the lateral direction. Note that our aspect ratios $H/2B$ were 0.42 for the longer plane of the rectangular tank and 0.63 for both the square tank and the shorter plane of the rectangular tank, and no secondary cell was observed.

The geometry of the primary circulation cells in each setup can be estimated by the ratio L_{CV}/L_{CH}, in which L_{CV}=vertical distance from the water surface to the center of the circulation cells and L_{CH}=the horizontal distance from the nozzle centerline to the center of the circulation cells (see Fig. 1). This ratio can also be interpreted as an approximate spreading of the surface jet.

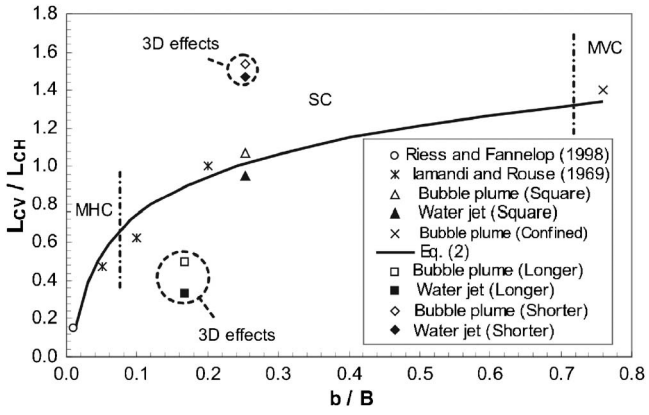

Fig. 9. Variation of the approximate spreading of the surface jet with the ratio of jet radius to tank radius (or half-width). Note that MHC, SC, and MVC correspond to the regions in which multiple horizontal cells, single cells, and multiple vertical cells are formed, respectively. Dashed circles indicate the data points obtained in the rectangular setup, where strong 3D effects were observed.

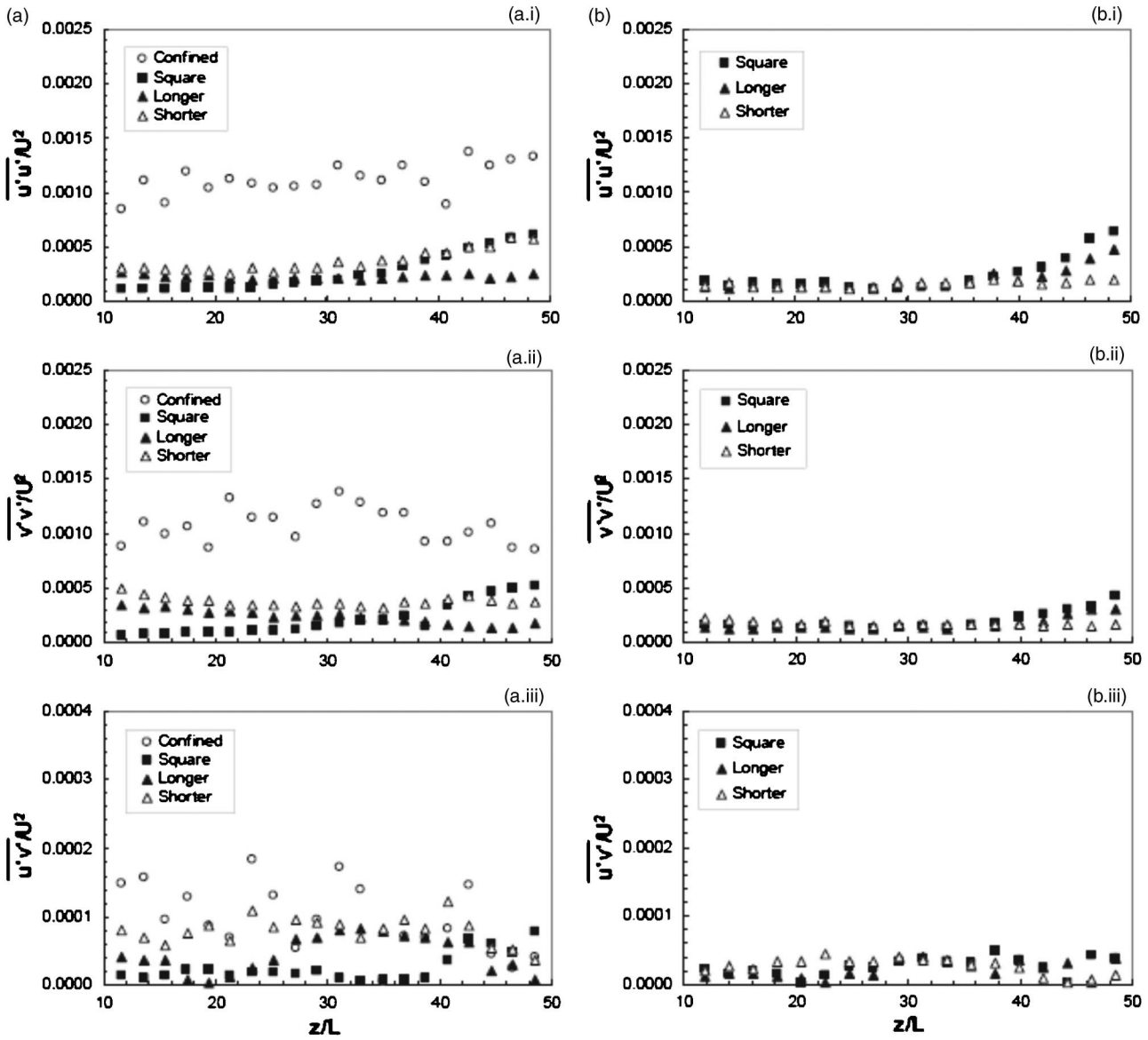

Fig. 10. Typical axial variation of the normalized turbulent stresses measured at $r=15$ cm ($Q_o=33.3$ cm^3/s) for (a) bubble plumes; (b) water jets: (i) horizontal normal stresses, (ii) vertical normal stresses, and (iii) shear stresses

The values of L_{CV}/L_{CH}, obtained from Figs. 7 and 8 are plotted in Fig. 9 along with the values from the literature. Fig. 9 shows that L_{CV}/L_{CH} increases logarithmically with b/B, which means that longer cells are formed in larger tanks. The curve shown in Fig. 9 [Eq. (2)] was also obtained from curve fitting ($r^2=0.964$) of experimental data

$$\frac{L_{CV}}{L_{CH}} = 0.675 \log\left(\frac{b}{B}\right) + 1.419 \tag{2}$$

It is interesting to observe that due to 3D effects in our rectangular tank, the values of L_{CV}/L_{CH} in the shorter and longer planes were about 1.5 and 0.4 times the value of L_{CV}/L_{CH} for the square tank, respectively (see Fig. 8). Besides, the values of L_{CV}/L_{CH} for bubble plumes are consistently higher than those for water jets, especially for the longer plane of the rectangular setup. This difference may be attributed to larger liquid volume fluxes (and perhaps higher turbulence levels) induced by the bubble plumes than those induced by the water jets (see Table 1), which may have caused higher spreading of the surface jet. It is consistent with the results of Fanneløp et al. (1991), in which the primary cell length was found to be a weak function of the flow rate in their bubble plume tests and independent of the flow rate in the water jet tests. This supports the negligibility of the densimetric Froude number, F, in Eq. (2). A diagram with approximate limits of b/B to estimate the flow patterns of the circulation cells based on the aspect ratios mentioned above is also given in Fig. 9. This diagram shows that multiple horizontal cells (MHC) are formed when b/B is up to about 0.1, single cells (SC) are formed when b/B ranges from about 0.1 and 0.7, and multiple vertical cells (MVC) are formed when b/B is larger than about 0.7. This suggests that Eq. (2) can be used to estimate both the size and number of circulation cells in a general tank.

Typical distributions of the normalized turbulent stresses $\overline{u'u'}/U^2$, $\overline{v'v'}/U^2$ and $\overline{u'v'}/U^2$ with the normalized vertical dis-

tance from the nozzle z/L are shown in Fig. 10, in which U and L=velocity and length scales given above, respectively. Note that the results are shown for values of z/L up to 50. For higher values of z/L, the turbulence levels increased significantly as the flow approached the surface jet region (at $z/L=60$). It can be seen that the horizontal normal stresses, $\overline{u'u'}/U^2$, were of the same order of the vertical normal stresses, $\overline{v'v'}/U^2$, and that the shear stresses, $\overline{u'v'}/U^2$, were much smaller than those, which implies that the turbulent flow field was nearly isotropic for all experiments. The turbulent stresses in the bubble plume tests were more affected by the tank geometry than those in the water jet tests. For example, in the bubble plume tests, the values of $\overline{v'v'}/U^2$ for the shorter plane of the rectangular setup were about two times larger than those for the longer plane, while in the water jet tests, the values were of the same order. The magnitude of the turbulent stresses for the bubble plumes in the square and rectangular setups was slightly higher than that for water jets. On the other hand, the magnitude of the turbulent stresses for bubble plumes in the confined setup was about three times higher than that in the square and rectangular setups due to the effect of the recirculation eddies. Moreover, these stresses did not decay with the inverse of axial distance, as expected for the turbulent stresses inside single-phase jets (see Rajaratnam 1976). The axial variation of the terms $u''u''$, $v''v''$ and $u''v''$, here referred to as periodic stresses, followed similar trends as those of turbulent stresses for both bubble plumes and water jets, but their magnitude was approximately twice as high.

An examination of the velocity signals in the entire tank (away from the jet/plume region) revealed that the periodic fluctuations were distributed approximately uniformly across the tank but their strength increased about one order of magnitude as the flow approached the center of the circulation cells. This behavior was similar for bubble plume and water jet tests. The flow fields at different times showed that the circulation cells traveled basically up and down within a distance of up to about 10 and 20% of water depth for the water jet and bubble plume tests, respectively. This was probably the cause of the wandering motions described by Eq. (1). The turbulent stresses were also distributed approximately uniformly across the tank. Nearly isotropic turbulence was obtained in the entire tank, with horizontal and vertical normal stresses within about 20% difference. Note that our measurements were limited to a distance of at least 4 cm from the walls.

Summary and Conclusions

An experimental study was conducted to investigate the effect of tank size and geometry on the ambient flow field and circulation patterns induced by circular bubble plumes and water jets. The results revealed a nonstationary nature of the flow for all experiments, which was attributed mainly to the presence of coherent structures instead of buoyancy-driven instabilities. The wandering frequency of the bubble plumes was assumed to be equal to the dominant frequency of the velocity oscillations near the bubble core. This frequency was found to increase with air flow rate and to decrease with tank size, and a correlation based on our measurements and results available in the literature was proposed to describe this variation.

The mean flow patterns clearly changed with tank geometry. While multiple vortices were stacked vertically for bubble plumes in the confined setup, a large-circulation flow cell surrounding the bubble plumes and water jets was generated in both the square and rectangular setups, but the latter produced strong 3D effects with larger flow entraining in the longer plane of the rectangular setup and smaller flow detraining in the shorter plane. These 3D effects were more pronounced in the bubble plume tests than in the water jet tests. A parameter corresponding to the spreading of the surface jet was introduced to describe the geometry of the circulation cells. This parameter was found to increase as the tank size became small compared to the radius of the jets and plumes, and a correlation was obtained to describe the flow patterns of the circulation cells as a function of tank size.

Nearly isotropic turbulent flow conditions were obtained in all experiments. However, the effect of tank size and geometry on the intensity of the turbulent stresses was more pronounced in the bubble plume tests. Besides, the axial variation of the turbulent and periodic stresses followed similar trends, but their magnitude was higher for bubble plumes in the confined setup than that in the square and rectangular setups because of the effect of the recirculation eddies.

The above results describe the ambient flow field and circulation patterns induced by bubble plumes and water jets, which are important in many engineering applications, including lake and reservoir aeration, mixing in wastewater treatment tanks, and prevention of suspended solids settling. It should be pointed out, however, that there are still a few important questions remaining. Our results imply that the wandering motion observed visually in the bubble plume experiments was caused mainly due to vertical oscillations in the position of the large circulation cells (instead of buoyancy-driven instabilities). The reason water jets are less susceptible to wandering motion is not clear, possibly due to much higher momentum flux in water jets. The reason for the 3D effects observed in the longer and shorter planes of the rectangular tank is also an open question. One possible explanation for such effects is the presence of secondary flows in the tank, as the surface jet in the shorter plane reaches the tank walls with higher velocity than that in the longer plane. Possible imbalanced Reynolds stresses and nonuniform distributions of wall shear stresses may also play an important role. Further research is needed to answer the above questions.

Acknowledgments

I.E.L.N. is supported by the Coordination for the Improvement of Higher Education Personnel Foundation (CAPES), Ministry of Education, Brazil. The writers are thankful to Perry Fedun and Chris Krath for building the experimental apparatus.

Notation

The following symbols are used in this technical note:

d_o = nozzle diameter (mm);
Q_a = volumetric air flow rate (cm^3/s);
Q_w = volumetric water flow rate (cm^3/s);
R = Reynolds number defined as $\mathsf{R}=U_o d_o/\nu$;
r = radial distance from the plume centerline (cm);
U_o = velocity at the nozzle exit for each phase (air or water) (m/s);
$\bar{u}$ = time-averaged horizontal velocity component (cm/s);
u' = turbulent horizontal velocity fluctuation (cm/s);
u'' = periodic horizontal velocity fluctuation (cm/s);
$\overline{u'u'}$ = horizontal normal stress due to turbulent fluctuations (cm^2/s^2);

J. Hydraul. Eng., 2008, 134(6): 833-842

$\overline{u''u''}$ = horizontal normal stress due to periodic fluctuations (cm^2/s^2);
$\overline{u'v'}$ = shear stress due to turbulent fluctuations (cm^2/s^2);
$\overline{u''v''}$ = shear stress due to periodic fluctuations (cm^2/s^2);
$\bar{v}$ = time-averaged vertical velocity component (cm/s);
v' = turbulent vertical velocity fluctuation (cm/s);
v'' = periodic vertical velocity fluctuation (cm/s);
$\overline{v'v'}$ = vertical normal stress due to turbulent fluctuations (cm^2/s^2);
$\overline{v''v''}$ = vertical normal stress due to periodic fluctuations (cm^2/s^2);
z = axial distance from the nozzle exit (cm); and
ν = kinematic viscosity of each phase (air or water) (m^2/s).

References

Abramovich, G. N. (1963). *The theory of turbulent jets*, MIT, Cambridge, Mass.

Bombardelli, F. (2004). "Turbulence in multiphase models for aeration bubble plumes." Ph.D. thesis, Dept. of Civil and Environmental Engineering, Univ. of Illinois at Urbana-Champaign, Ill.

Clift, R., Grace, J. R., and Weber, M. E. (1978). *Bubbles, drops, and particles*, Academic, New York.

Fanneløp, T. K., Hirschberg, S., and Küffer, J. (1991). "Surface current and recirculating cells generated by bubble curtains and jets." *J. Fluid Mech.*, 229, 629–657.

García, C. M., and García, M. H. (2006). "Characterization of flow turbulence in large-scale bubble–plume experiments." *Exp. Fluids*, 41(1), 91–101.

Iamandi, C., and Rouse, H. (1969) "Jet-induced circulation and diffusion." *J. Hydr. Div.*, 95(2), 589–601.

Jirka, G., and Harleman, D. R. F. (1979). "Stability and mixing of a vertical plane buoyant jet in confined depth." *J. Fluid Mech.*, 94, 275–304.

Lima Neto, I. E., Zhu, D. Z., and Rajaratnam, N. (2008). "Air injection in water with different nozzles." *J. Environ. Eng.*, 134(4), 283–294.

Mudde, R. F. (2005). "Gravity-driven bubbly flows." *Annu. Rev. Fluid Mech.*, 37, 393–423.

Rajaratnam, N. (1976). *Turbulent jets*, Elsevier Scientific, Amsterdam, The Netherlands.

Rensen, J., and Roig, V. (2001). "Experimental study of the unsteady structure of a confined bubble plume." *Int. J. Multiphase Flow*, 27(8), 1431–1449.

Riess, I. R., and Fanneløp, T. K. (1998). "Recirculation flow generated by line-source bubble plumes." *J. Hydraul. Eng.*, 124(9), 932–940.

Socolofsky, S. A. (2001). "Laboratory experiments of multiphase plumes in stratification and crossflow." Ph.D. thesis, MIT, Cambridge, Mass.

Soga, C. L. M., and Rehmann, C. R. (2004). "Dissipation of turbulent kinetic energy near a bubble plume." *J. Hydraul. Eng.*, 130(5), 441–449.